Nanoscale Horizons

ROYAL SOCIETY OF CHEMISTRY

COMMUNICATION

View Article Online
View Journal | View Issue

Cite this: *Nanoscale Horiz.*, 2021, 6, 568

Received 18th March 2021,
Accepted 30th April 2021

DOI: 10.1039/d1nh00152c

rsc.li/nanoscale-horizons

Simulated annealing fitting: a global optimization method for quantitatively analyzing growth kinetics of colloidal Ag nanoparticles†

Siyu Wu, ‡ Qinwei An‡ and Yugang Sun *

The involvement of heterogeneous solid/liquid reactions in growing colloidal nanoparticles makes it challenging to quantitatively understand the fundamental steps that determine nanoparticles' growth kinetics. A global optimization protocol relying on simulated annealing fitting and the LSW growth model is developed to analyze the evolution data of colloidal silver nanoparticles synthesized from a microwave-assisted polyol reduction reaction. Fitting all data points of the entire growth process determines with high fidelity the diffusion coefficient of precursor species and the heterogeneous reduction reaction rate parameters on growing silver nanoparticles, which represent the principal functions to determine the growth kinetics of colloidal nanoparticles. The availability of quantitative results is critical to understanding the fundamentals of heterogeneous solid/liquid reactions, such as identifying reactive species and reaction activation energy barriers.

New concepts

Real-time probing of colloidal nanoparticles' evolution kinetics in liquid solutions represents an emerging research area to understand the fundamental steps determining nanoparticle growth. The heterogeneous solid/liquid interfacial reactions responsible for growing nanoparticles in a closed system usually involve two primary interdependent functions, *i.e.*, diffusion of reactive precursor species and surface reactions of the precursor species on the growing nanoparticles. Many attempts have been made to develop *in situ* techniques for measuring nanoparticle evolution. It is still challenging to quantitatively determine the intrinsic parameters (*i.e.*, the diffusion coefficient of the precursor and the surface reaction rate constant) of the two intertwined functions. We apply the LSW model to describe nanoparticle growth with an autonomous ordinary differential equation that is challenging to fit to *in situ* measurements of low/moderate-density data points. A new concept of a global optimization protocol based on simulated annealing fitting is proposed to fit all data points of the entire growth process numerically. The fitting determines diffusion coefficients and surface reaction rate constants with high fidelity. The availability of intrinsic parameters' values offers the unprecedented opportunity to quantitatively understand the heterogeneous solid/liquid interfacial reactions of growing nanoparticles and rationally design the synthesis of colloidal nanoparticles.

We reported the measurement of growth kinetics of colloidal silver (Ag) nanoparticles in a microwave reactor using *in situ* high-energy X-ray diffraction (HEXRD), which was published in *Nano Letters* in 2016.[1] The availability of high-quality time-resolved HEXRD patterns offered the promise of quantifying the evolution kinetics of colloidal Ag nanoparticles in the course of reducing silver nitrate ($AgNO_3$) at elevated temperatures. The time-dependent mass evolution of the crystalline Ag nanoparticles exhibited sigmoidal shapes, and we mathematically fitted the data with a sigmoidal function, *i.e.*, $y = a\left[1 - \frac{1}{1 + e^{\left(\frac{x - x_0}{dx}\right)}}\right]$. The data fitting determined the constant parameters of a, x_0, and dx, which allowed us to conveniently compare the evolution kinetics under various reaction conditions (*e.g.*, different temperatures and different concentrations of $AgNO_3$). However, the condition-dependent constants derived from the pure mathematical fitting lacked physical meaning to represent the fundamental functions that determine the growth kinetics of colloidal nanoparticles. Professor Özkar and Professor Finke criticized this issue later in a paper published in *The Journal of Physical Chemistry C*,[2] in which they digitized our data and fitted the data with the Finke–Watzky (FW) two-step mechanism proposed by Professor Finke and Professor Watzky back in 1997.[3] The FW two-step mechanism consists of slow, continuous nucleation with a reaction rate constant of k_1 and autocatalytic surface growth with a reaction rate constant of

Department of Chemistry, Temple University, 1901 North 13th Street, Philadelphia, Pennsylvania 19122, USA. E-mail: ygsun@temple.edu

† Electronic supplementary information (ESI) available: Experiment details on the *in situ* experiment; full-version LSW model describing the growth kinetics of colloidal Ag nanoparticles; data processing and simulated annealing fitting of *in situ* experimental data; density functional theory calculations on Ag–PVP complexes. See DOI: 10.1039/d1nh00152c

‡ S. W. and Q. A. made equal contributions.

k_2. The mechanism is generally described in the format of serial (homogeneous) reactions as eqn (1):

$$\begin{aligned} &A \xrightarrow{k_1} B \\ &A + B \xrightarrow{k_2} 2B \\ &\text{net } A \rightarrow B \end{aligned} \tag{1}$$

where A and B stand for the precursor species and the composition species of the synthesized nanoparticles, respectively. Specifically, A represents Ag^+ ions and B represents Ag atoms of the growing Ag_n^0 nanoparticles in the aforementioned microwave-assisted synthesis of colloidal Ag nanoparticles. The rate law of the two-step reactions gives the time-dependent concentration of B, $[B]_t$, as a function of time, t, following

$$[B]_t = [A]_0\left[1 - \frac{k_1 + k_2[A]_0}{k_2[A]_0 + k_1 e^{(k_1+k_2[A]_0)t}}\right] \tag{2}$$

in which $[A]_0$ is the initial concentration of A. Eqn (2) provides a sigmoidal function to fit the data published in our 2016 *Nano Letters* paper. The fitting exercise determines the values of k_1 and k_2 with a fitting coefficient of determination (R^2) higher than 0.999, indicating the high quality of the data fitting. We respectfully appreciate Professor Özkar and Professor Finke for their fitting efforts, and we do not comment on the suitability of the FW two-step mechanism in describing the heterogeneous solid/liquid interfacial reactions involved in colloidal nanoparticle synthesis. The experimental HEXRD data reported in our 2016 *Nano Letters* paper primarily represent the growth kinetics of stable Ag nanoparticles because the nucleation process forms Ag nuclei that are too small (usually less than 2 nm) to give HEXRD signals. Therefore, we focus on analyzing the growth kinetics of colloidal Ag nanoparticles assuming that the nucleation process has ceased to produce new nuclei when decent HEXRD patterns start to be observed.

The models reported in the literature (including the FW two-step mechanism) describe the growth of colloidal nanoparticles as autocatalytic surface reactions.[2–6] Therefore, we believe that the mathematical equations describing the growth kinetics of colloidal nanoparticles should include the parameter of the surface area (equivalent to r^2) of the growing nanoparticles. For example, the model proposed by Lifshitz, Slyozov, and Wagner (LSW model) is well known to describe the growth of colloidal particles after nucleation.[5,6] In such a multiple-phase system, growing solid particles dispersed in a liquid solution containing precursor species depends on two consecutive processes, *i.e.*, the diffusion of precursor species to the surface of growing particles and the reaction of precursor species on the particles' surface (Fig. 1a).[7,8] When one of the two processes plays the decisive role in the growth kinetics of colloidal nanoparticles, the LSW model can be simplified to an asymptotic format, *i.e.*, either a surface reaction-limited model (Fig. 1b) or a diffusion-limited model (Fig. 1d).[6,9] The asymptotic models enable the feasibility to fit the *in situ* kinetic data of growing colloidal nanoparticles under well-controlled synthesis conditions,

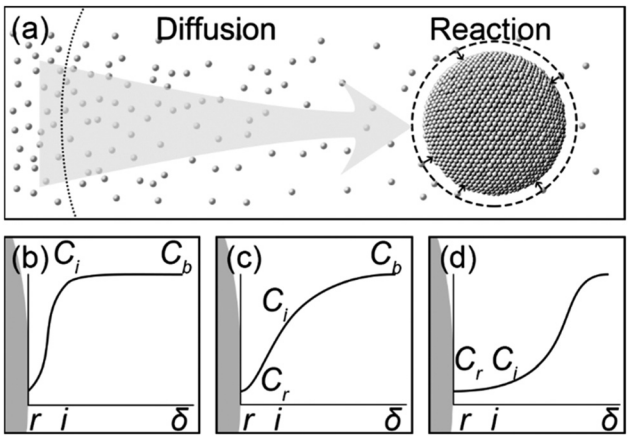

Fig. 1 (a) Schematic illustration of the LSW model responsible for the growth of colloidal Ag nanoparticles, showing the diffusion of appropriate Ag(I) precursor species across the diffusion layer (dotted circle) followed by reduction of the Ag(I) precursor on the growing Ag nanoparticles in the interfacial layer (dashed circle). (b–d) Concentration gradient profiles for different LSW approximations: (b) surface reaction-limited model, (c) full LSW model, and (d) diffusion-limited model. The length scale in (a–d) does not represent the true values.

leading to the determination of fundamental parameters such as the diffusion coefficient (D) of precursor species in the reaction solution and the reaction rate constant (k) of the precursor species on the growing nanoparticles' surface.[10–14] In most cases of colloidal nanoparticle synthesis, neither of the asymptotic models can accurately reflect the growth kinetics since both the diffusion of precursor species and surface reactions contribute comparably to determine the growth kinetics (Fig. 1c).[9] The full-version LSW model including the contributions of both diffusion and surface reactions has to be applied to fit the *in situ* measurement data to simultaneously determine D and k with acceptable fidelity. Because of the complexity of the kinetic equation, accurate determination of D and k from fitting the *in situ* data is still challenging.

In this Communication, we report the use of simulated annealing (SA) fitting to analyze *in situ* data throughout the entire growth of colloidal nanoparticles using the full-version LSW model and determine the values of both D and k with high fidelity. We use *in situ* data of synthesizing Ag nanoparticles in microwave-assisted polyol reduction of $AgNO_3$ (reported in our 2016 *Nano Letters* paper; ESI,† Section I) as an example to highlight the feasibility and accuracy of the SA fitting. In the synthesis, microwave heating was used to control the temperature of ethylene glycol (EG) solutions. Poly(vinyl pyrrolidone) (PVP) was added to serve as capping ligands to stabilize Ag nanoparticles. Successful determination of the values of fundamental kinetic parameters is promising to understand the thermodynamics and the active precursor species responsible for growing Ag nanoparticles. According to the LSW model shown in Fig. 1a (see the ESI,† Section II), the growth rate of the Ag nanoparticles is described as

$$\begin{cases} \dfrac{dr}{dt} = \dfrac{kD}{kr + D}\left(a - N_0 \cdot b \cdot r^3\right) \\ a = V_m \cdot C_0 \\ b = \dfrac{4\pi}{3V_s} \end{cases} \tag{3}$$

where r and t represent the radius of growing spherical Ag nanoparticles and time, and V_m, V_s, C_0, and N_0 stand for the molar volume of Ag metal (10.3 cm^3 mol^{-1}), the volume of reaction solution, the initial concentration of $AgNO_3$, and the number of growing Ag nanoparticles, respectively.

The autonomous ordinary differential equation (eqn (3)) can be solved numerically using the classic fourth-order Runge–Kutta method (RK4)[15] to give the nanoparticle growth trajectory $r(t)$ when the values of k and D are available, and an initial condition $r(t_0)$ is provided. On the other hand, when the nanoparticle growth trajectory $r(t)$ can be measured from *in situ* experiments, the values of k and D can be, in principle, determined by fitting the $r(t) \sim t$ data with eqn (3). In our 2016 paper the nanoparticle growth trajectory can be obtained from the total volume of Ag nanoparticles (V_{tot}), where $V_{tot} = \frac{4}{3}\pi r^3 N_0$ (see the ESI,† Section II, Fig. S2c). The average size of the as-synthesized Ag nanoparticles (r_{max}) after the complete reduction of $AgNO_3$ was determined using transmission electron microscopy (TEM) imaging. The complete reduction of $AgNO_3$ generated the maximum total volume of Ag nanoparticles (V_{tot}^{max}), which was calculated from the amount of $AgNO_3$ added to the reaction solution. The number of growing Ag nanoparticles (N_0) could be calculated accordingly. The values of a and b were defined for a given reaction system. Fitting eqn (3) to the experimental data is reduced to a three-parameter estimation problem about k, D, and $r(t_0)$. To avoid the uncertainty of the initial condition $r(t_0)$ that is close to zero, we applied the two-way RK4 method in which the initial condition $r(t_0)$ was set to the midpoint of the growth curve where the first derivative (*i.e.*, dV_{tot}/dt) reaches the maximum. Since the size at the midpoint $r(t_{mid})$ of stable growing nanoparticles is a fixed non-zero number in a given synthesis, the actual freedom of the numerical fitting becomes two. We have developed an extreme-condition model to determine k and D using the simplified asymptotic LSW models by focusing on the growth at the very early stage (reaction-limited model) and the very late stage (diffusion-limited model).[16] Because of the low density and small variation of experimental data points at the very early and the very late growth stages, the fidelity and accuracy of the fitted (k, D) values may be questionable. However, they can be used as the references as well as the initial guess for SA fitting to fit more experimental data points throughout the entire growth process, leading to improved fitting efficiency and saving computational time.

Since both k and D influence the growth rate of Ag nanoparticles, many different pairs of (k, D) can generate similar growth rates according to eqn (3) during the focused time periods, which results in a challenge to simultaneously determine the values of k and D with high fidelity from data fitting. We report the development of a global optimization fitting protocol that allows fitting all data points of the entire growth process to minimize the possible errors. Specifically, a SA method[17] allows a random search of the mathematically valid (k, D) pairs to determine the physically accurate (k, D) pair through statistical analysis. A C-program based on the SA algorithm is developed to determine the optimum (k, D) pairs that give the least sum of squared residuals (SSR) of V_{tot} between the theoretical fitting predictions (V_{fit}) and experimental curve (V_{exp}) at each data point measured at different time t_i (see the ESI,† Section III):

$$SSR = \sum_i \left| V_{fit}(t_i) - V_{exp}(t_i) \right|^2 \quad (4)$$

At the beginning of the algorithm, a random (k, D) pair is chosen as the starting point. The program will jump randomly to a new (k, D) pair in a neighboring region and check whether the SSR of the new iteration (n + 1) becomes smaller than the available record to give a better fit to the experimental data. The possibility of acceptance (P) of the new (k, D) pair relies on the Metropolis jumping rule.[18] A smaller SSR will be accepted immediately (P = 1), and a larger SSR will be accepted with the condition:

$$P(k, D) = \begin{cases} 1, SSR_{n+1} < SSR \\ \exp\left(-\dfrac{|SSR_{n+1} - SSR|}{R\tau}\right), SSR_{n+1} \geq SSR \end{cases} \quad (5)$$

in which R is a constant that is only related to the efficiency of the algorithm, and τ is the current "temperature" of the SA process in analogy to metallurgical processes. The value of τ decreases after each iteration of the search, and the neighboring region for picking a new (k, D) pair narrows accordingly. A continuous search leads to a convergence of the (k, D) trace in the k–D plane to a point that possibly has the smallest SSR. Due to the Monte-Carlo feature (*i.e.*, randomness and probability) of the SA algorithm, the best fitting result becomes more likely to be reached as the program runs for enough time and iteration cycles. In practice, the program is forced to stop when a set of criteria are fulfilled (*e.g.*, the "temperature" of annealing is lower than τ_{min}), avoiding possible overfitting and saving data processing time.

Fig. 2(a) presents the (k, D) results from fitting the experimental data of growing Ag nanoparticles at 160 °C by repeating the SA program for 100 cycles. The (k, D) pair determined with the extreme-condition model was used as the starting point for the SA fitting. The likely optimized (k, D) pairs scatter around one of the branches of the rectangular hyperbola, *i.e.*, $H = kD/(kr_i + D)$ with both r_i and H constants, in the k (horizontal)–D (vertical) plane. The (k, D) pairs with the smallest SSRs (red dots, Fig. 2a) cluster in a confined region, highlighting the feasibility to determine high-fidelity values of k and D. The distribution of k is very narrow (*i.e.*, 2.5–3.1 × 10^{-7} m s^{-1}) while the values of D scatter in a wider range (*i.e.*, 5–10 × 10^{-14} m^2 s^{-1}), suggesting that k can be more accurately determined than D. Such a difference indicates that the contribution of surface reactions to the growth kinetics of Ag nanoparticles at 160 °C is more determining than the contribution of precursor diffusion. Considering that the SA algorithm suggests the uncertainty of the fitting results, we use the averages of the top 10% results from 100 cycles of SA fitting to improve the accuracy. The statistical accuracy of k evaluated from the clustered (k, D) pairs with the smallest SSRs is higher than that of D, *i.e.*, (2.87 ± 0.052) × 10^{-7} m s^{-1} for k with a statistical deviation of

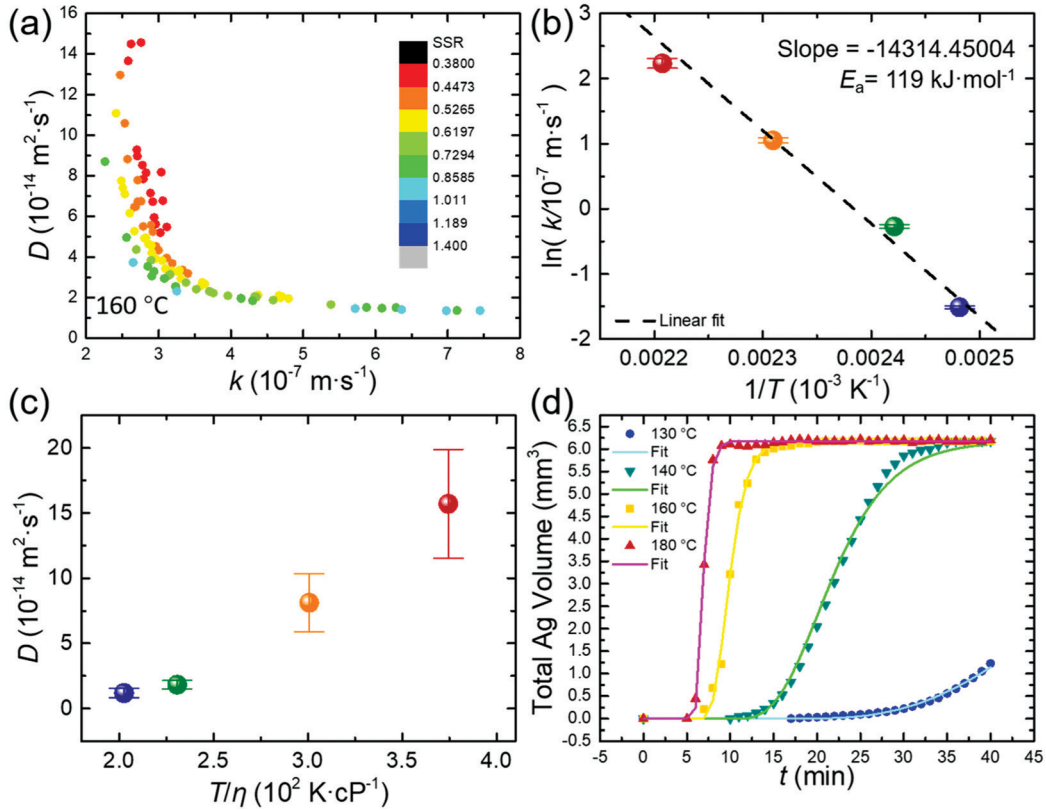

Fig. 2 (a) The optimized (*k*, *D*) pairs determined from the SA fitting of the growth kinetics of colloidal Ag nanoparticles measured from the synthesis at 160 °C. The concentration of $AgNO_3$ was 0.1 M and the concentration of PVP in terms of repeat units was 0.15 M. The colors of the dots correspond to the SSRs calculated between the experimental data and the fitting data. (b) Plot of ln(*k*) as a function of 1/*T*. (c) Dependence of *D* on T/η. (d) Plots of the fitted kinetic curves and the measured data (symbols) of the syntheses at different temperatures: 130 °C (blue, ●), 140 °C (green, ▼), 160 °C (yellow, ■), and 180 °C (red, ▲).

18% *versus* $(8.13 \pm 2.24) \times 10^{-14}$ m^2 s^{-1} for *D* with a statistical deviation of 28%. It is worth pointing out that the (*k*, *D*) pairs with the smallest SSRs derived from the SA fitting cluster at the upper arm of the half hyperbola to highlight the more reaction-limited growth of Ag nanoparticles. Such a conclusion is consistent with $kr_{max}/D < 1$, which is calculated using the fitted (*k*, *D*) values (see the ESI,† Table S2).

The growth kinetics of Ag nanoparticles accelerates significantly with the reaction temperature. SA fitting reveals that increasing temperature leads to the increase of both the diffusion of the Ag(I) precursor and the surface reduction of Ag(I) precursor species on growing Ag nanoparticles. The values of *k* and *D* of the syntheses at varying temperatures, *e.g.*, 130 °C, 140 °C, 160 °C, and 180 °C, are presented in Table S2 (see the ESI†). When the temperature increases from 130 °C to 180 °C, *k* increases by 42.4 times from 0.22×10^{-7} m s^{-1} to 9.33×10^{-7} m s^{-1}. The logarithm of the temperature-dependent reaction rate constant (*i.e.*, ln *k*) exhibits a linear relationship with the reciprocal of the thermodynamic temperature (1/*T*) (Fig. 2b). According to the Arrhenius equation $k = Ae^{-E_a/RT}$ (*R* and *A* represent the universal gas constant and the frequency factor), the activation energy (E_a) of reducing the Ag(I) precursor on growing Ag nanoparticles in EG is calculated to be 119.0 kJ mol^{-1}.

The clustering center of the *D* values increases by 13.2 times from 1.19×10^{-14} m^2 s^{-1} to 1.57×10^{-13} m^2 s^{-1} as the temperature increases from 130 °C to 180 °C (Fig. 2c, Table S2, see the ESI†). According to the Stokes–Einstein equation, $D = \frac{k_B T}{6\pi\eta r_{dy}}$, the diffusion coefficient (*D*) of a dynamic spherical molecule is proportional to temperature (*T*) and inversely proportional to the viscosity (η) of the solvent and the dynamic radius of the diffusive molecule (r_{dy}). Fig. 2c shows the dependence of *D* derived from the SA fitting on T/η, in which the temperature-dependent viscosity of a PVP–EG solution is adjusted according to the reported data.[19] The plot is linear despite the first data point being collected at 130 °C, where the growth curve is incomplete and may not represent the true *D* value. The accuracy of the values of *k* and *D* determined from the SA fitting can be evaluated by comparing the theoretical growth kinetics calculated from eqn (3) with the experimental growth kinetics. The good agreement is shown in Fig. 2d, highlighting the high fidelity of the SA fitting in determining *k* and *D*.

The SA fitting is also applied to analyze the growth kinetics of colloidal Ag nanoparticles synthesized with different concentrations (C_0 = 0.05 M, 0.10 M, and 0.15 M) of $AgNO_3$ at a constant temperature of 160 °C and a constant concentration of

PVP (0.15 M) (Fig. 3a). The values of k and D determined from these syntheses are presented in Table S3 (see the ESI†). The diffusion coefficient of reactive precursor species, D, remains essentially constant around $\sim 10 \times 10^{-14}$ m^2 s^{-1} (Fig. 3b), which is consistent with the Stokes–Einstein equation. In contrast, the fitted surface reaction rate constant, k, decreases from 6.21×10^{-7} m s^{-1} to 2.12×10^{-7} m s^{-1} as the concentration of $AgNO_3$ increases from 0.05 M to 0.15 M (Fig. 3c). According to the Arrhenius equation, the surface reaction rate constant should not vary with the precursor concentration at a constant temperature. The deviation of the fitted k and the expected k implies that the actual precursor involved in the surface reduction for growing Ag nanoparticles is not $AgNO_3$ (or Ag^+).

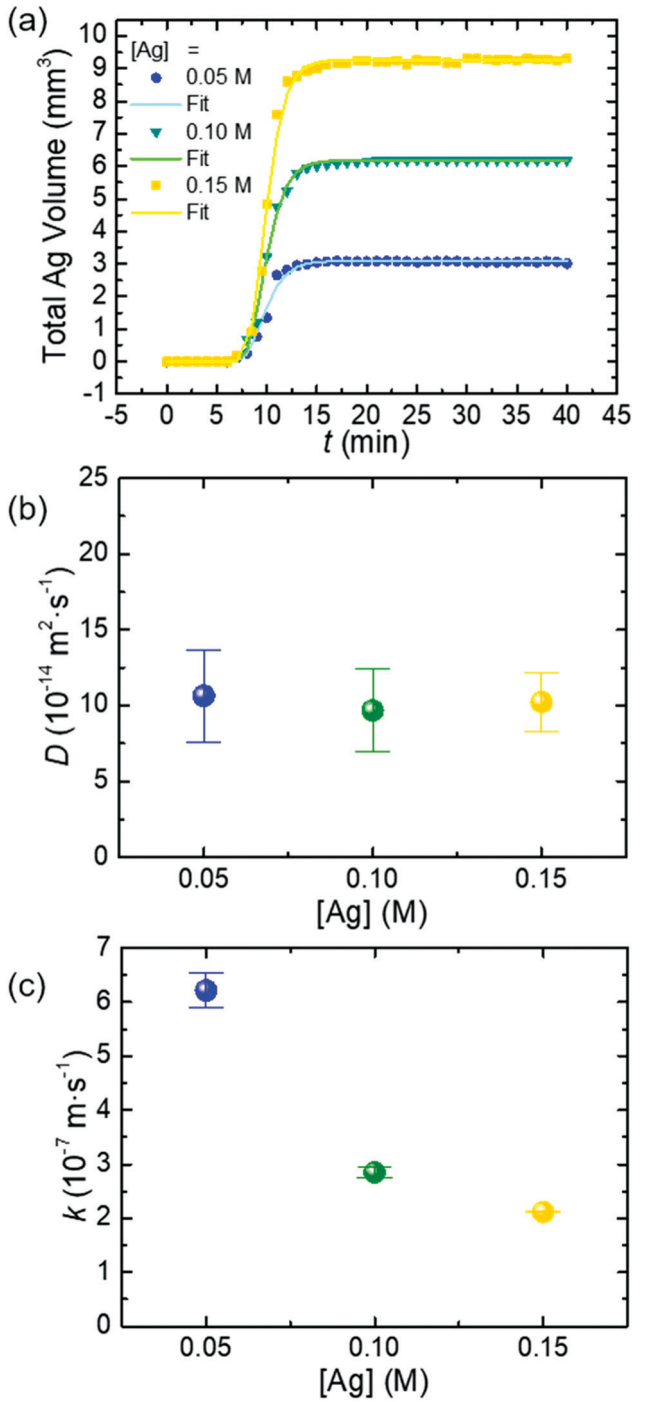

Fig. 3 Analysis of time-resolved HEXRD patterns recorded in the growth of colloidal Ag nanoparticles at different $AgNO_3$ concentrations: 0.05 M (blue, ●), 0.10 M (green, ▼), and 0.15 M (yellow, ■). (a) Total Ag volume as a function of time (symbols) at different $AgNO_3$ concentrations and their corresponding theoretical calculation (curves) using the SA fitting. (b) Diffusion coefficient (D) at different $AgNO_3$ concentrations. (c) Reaction rate constant (k) at different $AgNO_3$ concentrations.

We have performed basic density functional theory (DFT) calculations on the interactions between Ag^+ ions (or Ag^0 atoms) and the vinylpyrrolidone (VP) repeat unit (see the ESI,† Section IV). The calculation results show that the linear coordination of Ag ions to the carbonyl groups of VP units is thermodynamically favorable (see the ESI,† Fig. S7), which is consistent with claims proposed in a previous report.[20] The formation of the Ag^+–O–VP complex enriches the electron densities on the Ag^+ ions due to electron donation of the pyrrolidone ring, benefiting the reduction of Ag(I) to metallic Ag.[21] Therefore, the actual precursor species involved in the surface reaction is the Ag^+–O–VP complex rather than all Ag(I) species that are used in the SA fitting. According to the LSW model, the consumption rate of Ag(I) species due to the surface reaction on growing Ag nanoparticles is described as (eqn (S2), see the ESI†):

$$J_{\mathrm{rxn}} = 4\pi r^2 k(C_i - C_r) \approx 4\pi r^2 k \cdot C_i \qquad (6)$$

where C_i represents the concentration of the Ag(I) precursor at the imagined solid/liquid interface i (the dashed circle in Fig. 1a). C_r is the concentration of the Ag(I) precursor near the surface of a Ag nanoparticle, which is equal to the negligibly low solubility of the Ag atoms under the reaction conditions. For growing Ag nanoparticles with a radius of r, $k_{\mathrm{fit}} C_{i,\mathrm{total\ Ag(I)}} = k_{\mathrm{actual}} C_{i,\mathrm{Ag^+–O–VP}}$, in which k_{fit} is the rate constant (shown in Fig. 3c) determined from the fitting process using the concentration of total Ag(I) in bulk solution, and k_{actual} stands for the rate constant corresponding to the actual reaction precursor of the Ag^+–O–VP complex. This equation is rewritten as

$$\frac{C_{i,\mathrm{Ag^+-O-VP}}}{C_{i,\mathrm{totalAg(I)}}} = \frac{k_{\mathrm{fit}}}{k_{\mathrm{actual}}} \qquad (7)$$

The left term represents the fraction of Ag^+ coordinated with PVP. When the concentration of PVP is constant, a higher concentration of $AgNO_3$ gives a lower $\frac{C_{i,\mathrm{Ag^+-O-VP}}}{C_{i,\mathrm{totalAg(I)}}}$ at constant temperature. Since the principle k_{actual} is constant at a given temperature, the value of k_{fit} determined from the SA fitting is smaller at a higher concentration of $AgNO_3$, which is observed in Fig. 3c.

Conclusions

In summary, a global fitting method based on the SA algorithm has been developed to fit the experimentally measured growth

kinetics of colloidal nanoparticles using the full-version LSW model. The fitting applies to all data points throughout the entire growth process determined by both the surface reaction and diffusion of precursor species, resulting in the extraction of reliable k and D. According to the principle of the LSW model, the presented fitting protocol readily applies to the synthesis of colloidal nanoparticles, in which continuous growth of colloidal nanoparticles is supported by the surface reaction after burst nucleation. Availability of the fundamental kinetic parameters, k and D, is crucial to understand the insightful details of nanoparticle growth. For example, the precursor species involved in the surface reaction on growing Ag nanoparticles is suggested as the Ag^{+}–O–VP complex. The activation energy of the surface reduction of the Ag^{+}–O–VP complex on growing Ag nanoparticles is 119.0 kJ mol^{-1}. The global fitting and quantitative understanding of the growth kinetics of colloidal nanoparticles provide a promising strategy for understanding the in-depth mechanism of surface reactions on growing nanoparticles.

Conflicts of interest

There are no conflicts to declare.

Acknowledgements

This work was supported by the National Science Foundation under NSF award 1946912. We thank Prof. Spiridoula Matsika for the tutoring and guidance on the DFT calculations.

References

1 Q. Liu, M. R. Gao, Y. Liu, J. S. Okasinski, Y. Ren and Y. Sun, *Nano Lett.*, 2016, **16**, 715–720.
2 S. Özkar and R. G. Finke, *J. Phys. Chem. C*, 2017, **121**, 27643–27654.
3 M. A. Watzky and R. G. Finke, *J. Am. Chem. Soc.*, 1997, **119**, 10382–10400.
4 J. D. Martin, *Chem. Mater.*, 2020, **32**, 3651–3656.
5 I. M. Lifshitz and V. V. Slyozov, *J. Phys. Chem. Solids*, 1961, **19**, 35–50.
6 C. Wagner, *Ber. Bunsen-Ges. Phys. Chem.*, 1961, **65**, 581–591.
7 T. Sugimoto, *Monodispersed Particles*, Elsevier, Amsterdam, NL, 2001.
8 N. T. Thanh, N. Maclean and S. Mahiddine, *Chem. Rev.*, 2014, **114**, 7610–7630.
9 R. Viswanatha, P. K. Santra, C. Dasgupta and D. D. Sarma, *Phys. Rev. Lett.*, 2007, **98**, 255501.
10 H. Zheng, R. K. Smith, Y. W. Jun, C. Kisielowski, U. Dahmen and A. P. Alivisatos, *Science*, 2009, **324**, 1309–1312.
11 J. M. Yuk, J. Park, P. Ercius, K. Kim, D. J. Hellebusch, M. F. Crommie, J. Y. Lee, A. Zettl and A. P. Alivisatos, *Science*, 2012, **336**, 61–64.
12 J. Lee, J. Yang, S. G. Kwon and T. Hyeon, *Nat. Rev. Mater.*, 2016, **1**, 16034.
13 H. G. Liao, D. Zherebetskyy, H. Xin, C. Czarnik, P. Ercius, H. Elmlund, M. Pan, L. W. Wang and H. Zheng, *Science*, 2014, **345**, 916–919.
14 Y. Sun, X. Zuo, S. Sankaranarayanan, S. Peng, B. Narayanan and G. Kamath, *Science*, 2017, **356**, 303–307.
15 C. Runge, *Math. Ann.*, 1895, **46**, 167–178.
16 S. Wu and Y. Sun, *Nano Res.*, 2019, **12**, 1339–1345.
17 T. J. P. Penna, *Comput. Phys.*, 1995, **9**, 341–343.
18 B. Gidas, in *Topics in Contemporary Probability and Its Applications*, ed. J. L. Snell, CRC, Boca Raton, FL, 1995, ch. 7, 159–232.
19 W. Yu, H. Xie, L. Chen and Y. Li, *Powder Technol.*, 2010, **197**, 218–221.
20 X. Xia, J. Zeng, L. K. Oetjen, Q. Li and Y. Xia, *J. Am. Chem. Soc.*, 2012, **134**, 1793–1801.
21 C. Wu, B. P. Mosher, K. Lyons and T. Zeng, *J. Nanosci. Nanotechnol.*, 2010, **10**, 2342–2347.

Electronic Supporting Information

Simulated Annealing Fitting: A Global Optimization Method for Quantitatively Analyzing Growth Kinetics of Colloidal Nanoparticles

*Siyu Wu, Qinwei An, and Yugang Sun**

Department of Chemistry, Temple University, 1901 North 13th Street, Philadelphia, Pennsylvania 19122, USA

Supporting information to DOI: 10.1039/x0xx00000x

Section I: In situ experiment details on the synthesis of Ag nanoparticles

A in situ microwave reactor compatible with the high-energy synchrotron x-ray beamline was used to probe the evolution of colloidal Ag nanoparticles from microwave-assisted polyol reduction of silver nitrate at controlled temperatures. The recorded time-dependent high-energy x-ray diffraction (HEXRD) patterns were reported in our previous *Nano Letters* paper published in 2016.[1] The experimental details are described in the following.

Chemicals and synthesis. Silver nitrate ($AgNO_3$), ethylene glycol (EG), polyvinylpyrrolidone (PVP, $M_w \approx 55\,000$, K-30) were purchased from Sigma-Aldrich. In the synthesis, microwave heating was used to control the temperature of reaction solution. PVP was used as surface capping ligands to stabilize the synthesized Ag nanoparticles. Colloidal Ag nanoparticles were synthesized from the reduction of $AgNO_3$ in EG at elevated temperatures. In a typical synthesis, a 6-mL EG solution containing 0.10 M $AgNO_3$ and 0.15 M PVP (based on the repeating unit) was loaded to a 10-mL microwave reaction vessel. The reaction mixture was heated by microwave radiation from room temperature to a desired temperature (e.g., 130 °C, 140 °C, 160 °C, 180 °C in the experiment)

at a temperature ramp rate of ~20 °C/min, and the temperature was then maintained at the desired temperature for 35 minutes to complete the growth of Ag nanoparticles. After synthesis, the reaction solution was quickly cooled by flowing the pressurized air.

Instrumentations. **Figure S1** shows a schematic illustration of the in situ experiment setup. The in situ microwave reactor was placed at 1 ID-E beamline at the Advanced Photon Source (APS), Argonne National Laboratory (ANL), which provided an incident x-ray beam with a photon energy of 70 keV (wavelength = 0.1771 Å) for the experiment. [Note: This research used resources of the Advanced Photon Source, a U.S. Department of Energy (DOE) Office of Science User Facility, operated for the DOE Office of Science by Argonne National Laboratory under Contract No. DE-AC02-06CH11357.] The in situ microwave reactor was modified with a commercial Monowave 300 reactor (Anton Paar). The direct x-ray beam was blocked by a beam stopper with size of 0.3 mm × 0.3 mm, and the scattered x-ray signals were collected by an array of four GE 41RT detector at the frequency of 1 pattern per minute. Transmission electron microscope (JEOL 2100F) was used to characterize morphology, size, and size distribution of the as-synthesized Ag nanoparticles.

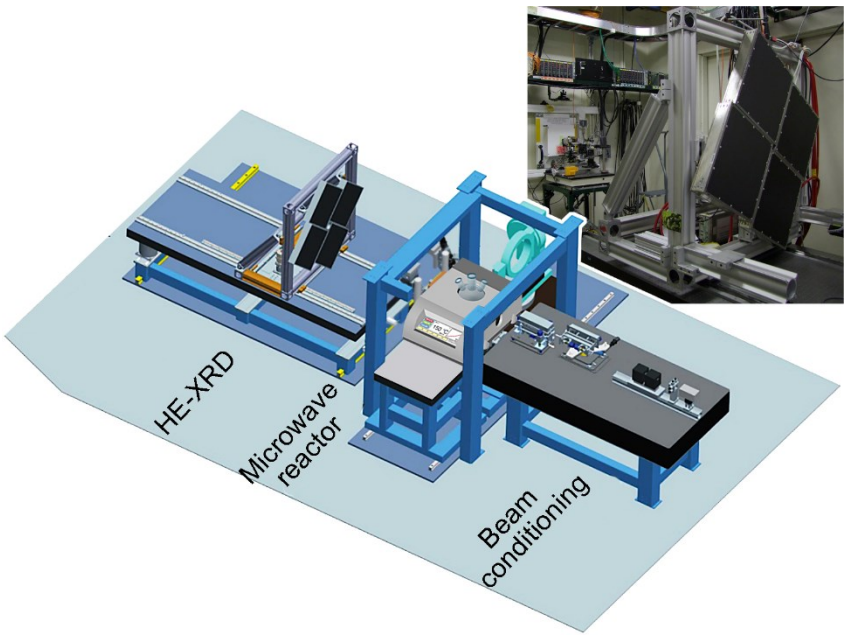

Figure S1. Scheme illustration of the in situ experiment setup.

Section II: Full-version LSW model of growing colloidal Ag nanoparticle

In the formation of Ag nanoparticles from reduction of $AgNO_3$, the reduction of Ag(I) for a period of time at an appropriate temperature accumulates a high enough concentration (i.e., high supersaturation) of Ag^0 atoms to trigger a spontaneous formation of solid Ag nuclei. In general, the growth of nuclei quickly consumes Ag^0 atoms to lower its supersaturation, resulting in a cease of nucleation that requires a high supersaturation of Ag^0 atoms. Once the stable nuclei are formed in the solution, heterogeneous reduction of precursor Ag(I) species on the surfaces of nuclei becomes favorable to enlarge the nuclei into nanoparticles with desirable sizes because this growth process is thermodynamically favorable. Therefore, the instantaneous nucleation and evolutionary growth steps are well separated to determine the synthesis of colloidal nanoparticles.

The heterogeneous solid/liquid reduction reaction represents one of the crucial step to determine the growth kinetics of colloidal Ag nanoparticles. Because the precursor Ag(I) species is supplied in solution phase and the reduction reaction occurs on the surface of growing Ag nanoparticles, diffusion of the precursor Ag(I) species to the nanoparticle surface is also important to determine the growth kinetics of Ag nanoparticles. The LSW model represents the well-accepted model describing growth kinetics of nanoparticles, i.e., enlargement rate of the nanoparticles as a function of growth time. In the LSW model, the consumption rate of the Ag(I) precursors (J_{rxn}) is equal to the supply rate of diffusion flux (J_{diff}), which supports the growth of Ag nanoparticles (Figure 1a, main text). The corresponding enlargement rate of growing Ag nanoparticles will be

$$\frac{4\pi r^2}{V_m} \cdot \frac{dr}{dt} = J_{rxn} = J_{diff} \qquad \text{(S1)}$$

in which V_m, t, and r are the molar volume of Ag metal, the growth time, and radius of the growing Ag nanoparticle at time t, respectively. If the surface reduction of precursor Ag(I) species is assumed to be first order with respect to both the precursor Ag(I) species and the surface of growing Ag nanoparticle, the consumption rate J_{rxn} of a spherical nanoparticle can be represented by:

$$J_{rxn} = k \cdot 4\pi r^2 \cdot (C_i - C_r) \qquad \text{(S2)}$$

C_i represents the concentration of the precursor Ag(I) species at the imaginary solid/liquid interface i (the dashed circle in Figure 1a). C_r is the concentration of the precursor Ag(I) species at the solid surface of the nanoparticle, which is equal to the solubility of Ag atoms and is negligibly small

under the reaction conditions. k represents the heterogeneous reaction rate constant of reducing the precursor Ag(I) species on the Ag nanoparticle surface. Meanwhile, the diffusion of Ag(I) precursor is assumed to follow the Fick's first law that can described by:

$$J_{diff} = \frac{4\pi Dr(r+\delta)}{\delta}(C_b - C_i) \approx 4\pi Dr(C_b - C_i), \text{ when } \delta \gg r \quad \text{(S3)}$$

in which D, δ, and C_b stand for diffusion coefficient, diffusion layer thickness, and bulk solution concentration of Ag(I) precursor species. A general description of the enlargement rate of a single Ag nanoparticle can be expressed by combining eq. (S1-S3):

$$\frac{dr}{dt} = \frac{kD}{kr+D} V_m (C_b - C_r) \approx \frac{kD}{kr+D} V_m C_b, \text{ when } C_b \gg C_r \quad \text{(S4)}$$

The reduction of Ag(I) precursor to grow Ag nanoparticles consumes the Ag(I) precursor in the bulk solution, leading to a monotonous decrease of C_b:

$$C_b = C_0 - \frac{V_{Ag,\,total}}{V_m \cdot V_s} \quad \text{(S5)}$$

where C_0 is the initial concentration of the Ag(I) precursor (i.e., the concentration of $AgNO_3$), V_s is the volume of the reaction solution, and $V_{Ag,total}$ is the total volume of the solid Ag nanoparticles. It is reasonable to assume that the number of the Ag nanoparticles remains constant as N_0 during the nanoparticle growth after the nucleation, since the burst nucleation stops immediately after the supersaturation level of the solution decreases significantly. Therefore, when Ag nanoparticles in a reaction system enlarges to a radius of r, the concentration of the Ag(I) precursor remaining in bulk solution (C_b) becomes:

$$C_b = C_0 - \frac{N_0 \frac{4}{3}\pi r^3}{V_m \cdot V_s} \quad \text{(S6)}$$

Therefore, eq. (S4) can be further reduced to:

$$\frac{dr}{dt} = \frac{kD}{kr+D} V_m \left[C_0 - \frac{4N_0\pi}{3V_m \cdot V_s} r^3 \right] = \frac{kD}{kr+D}\left(a - N_0 \cdot b \cdot r^3\right) \quad \text{(S7)}$$

in which $a = V_m \cdot C_0$ and $b = \frac{4\pi}{3V_s}$. The constant a and b can be calculated using V_m of 10.3 $cm^3\ mol^{-1}$ and the values of C_0 and V_s for a synthesis solution. This autonomous ordinary differential equation describes the growth rate (dr/dt) as a function of the radius of an individual nanoparticle (r). If the ensemble of nanoparticles follows a size distribution that a total number (N_0) of nanoparticles have a volume-weighted average size of $\bar{r}$:

$$\bar{r} = \left(\frac{3 \; V_{Ag,\,tot}}{4\pi \quad N_0} \right)^{\frac{1}{3}} \tag{S8}$$

Eq. (S7) can be rewritten as the change rate of total Ag particle volume ($dV_{Ag,tot}/dt$) as a function of the Ag particle volume by substituting r with $V_{Ag,tot}$. Eq. (S7) is so-called the "full-version" LSV growth model because it includes contributions of both diffusion and surface reaction.

Section III: Data processing and simulated annealing fitting of experimental data

Data pretreatment. The experimental data of growing colloidal Ag nanoparticles was adopted from our previous work.[1] The 2D pattern recorded by the x-ray detector was calibrated with a standard LaB_6 sample and unreacted reaction mixtures. The 2D ring pattern was then reduced to 1D HEXRD pattern using Fit2D software. The as-synthesized Ag particles exhibited HEXRD patterns of a typical face-centered cubic (*fcc*) lattice, showing (111), (200), and (220) peaks at 4.3°, 5.0°, and 7.0° (**Figure S2**a). Because of the high crystallinity of the Ag nanoparticles, the peak area of HEXRD patterns is proportional to the amount (or volume) of the Ag nanoparticles, which can be determined by referencing with the HEXRD pattern of Ag nanoparticles formed from a complete reduction of the Ag(I) precursor. The (111) peak area integrated from 4.2° to 4.4° is used to calculate the total amount (or particle volume) of growing Ag nanoparticles (Figure S2b). Complete reduction of 0.1 M $AgNO_3$ in 6-mL solution formed 6.18 mm^3 of Ag at the longest reaction time (i.e., in the plateau region in Figure S2c). The time-dependent data points are converted to the total volumes (V_{tot}/mm^3), which were fitting with the simulated annealing program. The time-dependent peak area of (200) peaks are also presented for comparison (Figure S2d).

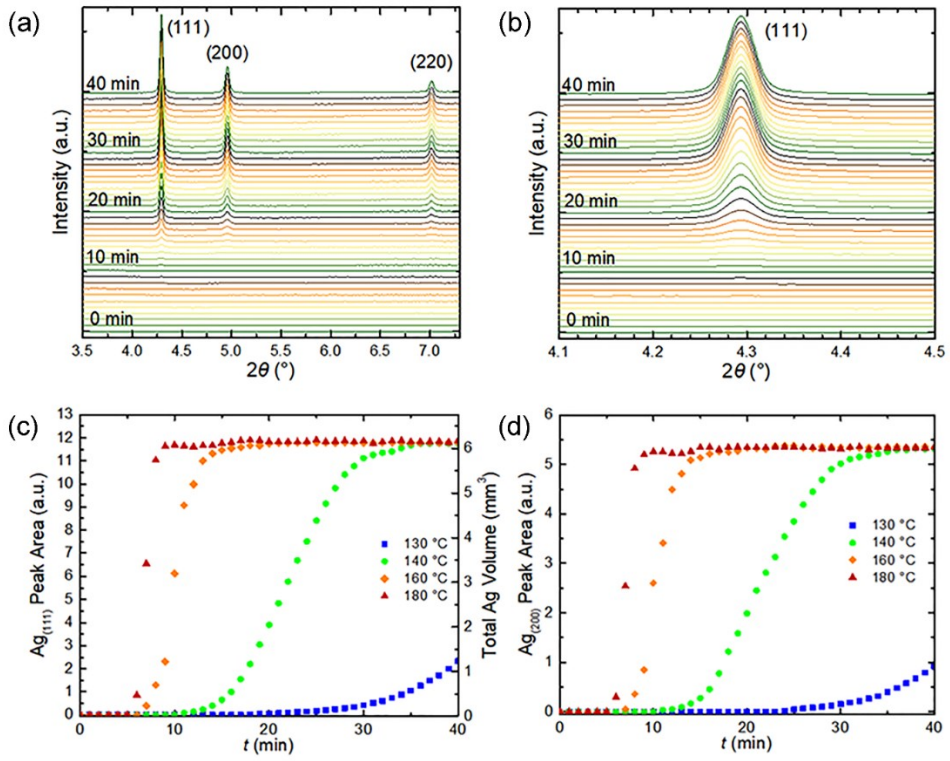

Figure S2. (a) HEXRD patterns of the reaction solution for synthesizing colloidal Ag nanoparticles at 140 °C in the in situ microwave reactor. The time interval for recording the HEXRD patterns was 1 minute. (b) Blowup of the (111) peaks. (c) Integrated (111) peak areas of the syntheses at different temperatures: 130 °C (blue, ■), 140 °C (green, ●), 160 °C (orange, ♦), and 180 °C (red, ▲). The time-dependent peak areas were converted to the total volume of growing Ag nanoparticles ($V_{Ag,tot}$, right axis). (d) Integrated (200) peak areas of the syntheses at different temperatures.

It is worthy of pointing out that the sensitivity of the in-situ HEXRD is not high enough to probe the formation of Ag nuclei and their growth at the very early stage when the total volume of the growing Ag nanoparticles is less than ~1% of V_{max} (or <~0.06 mm^3). The Ag nanoparticles formed at the nucleation stage and early growth stage (t_{exp} < 10 min) are small in size and lack of long-range order of crystallinity to exhibit HEXRD patterns with a reasonable signal-to-noise ratio. The lateral dimensions of Ag nanoparticles along Ag[111] and Ag[200] directions can also be estimated from the full width at half maximum (FWHM) of the corresponding peaks of in situ HEXRD patterns using Scherrer equation. Although the lateral dimension along Ag[111] expands slightly faster than that along Ag[200] at the early stage, the expansion of Ag nanoparticles along both directions shows similar sigmoidal profiles (Figure S3c-d), indicating a general isotropic growth throughout the entire synthesis. Therefore, the maximum lateral dimensions at the longest reaction time can be used as the diameters of the nanoparticles to calculate N_0 according to $N_0 = V/(\frac{4}{3}\pi r^3)$. The time-dependent evolution of the total volume of Ag nanoparticles ($V_{tot}(t)$) using $V_{tot}(t) = \frac{4}{3}\pi r^3(t) \cdot N_0$.

Initial estimation of k and D using the extreme-condition model. A proper initial guess of the values of k and D can significantly improve the performance of the simulated annealing algorithm and increase the efficiency to reach a converged result since it helps narrow the searching zone to a reasonable magnitude. The extreme-condition model from our previous work[2] was applied to obtain the initial guess of the values of k and D from a growth curve. The initial guess of the k value can be obtained from the slope of the $V_{tot}^{1/3}$ vs t plot at the very beginning stage (**Figure S3**a):

$$\left.\frac{d(V_{tot}^{1/3})}{dt}\right|_{\bar{r} \ll \bar{r}_{max}} = \left(\frac{4\pi N_0}{3}\right)^{1/3} ka \tag{S9}$$

and the D value can be obtained from the slope of the $\ln(V_{tot,max}^{1/3} - V_{tot}^{1/3})$ vs t plot at the very late stage (Figure S3b):

$$\left.\frac{d\left[\ln\left(V_{tot,max}^{1/3} - V_{tot}^{1/3}\right)\right]}{dt}\right|_{\bar{r} \to \bar{r}_{max}} = -3\left(a^2 \cdot b \cdot N_0\right)^{\frac{1}{3}} \cdot \frac{kD}{k\bar{r}_{max} + D} \tag{S10}$$

a and b are constants that only related to the synthesis condition, i.e., $a = V_m \cdot C_0$ and $b = \frac{4\pi}{3V_s}$. The initial estimations of k and D for the synthesis at different temperatures are listed in **Table S1**. It is worthy of pointing out that the extreme condition model focusing only on the two special stages is not able to determine the accurate values of k and D , particularly when the temporal resolution of data collection is low and the data value variation rate is small. Despite of the challenge, the values of k and D can be used as the starting point for the simulated annealing fitting that relies on all data points of the entire growth.

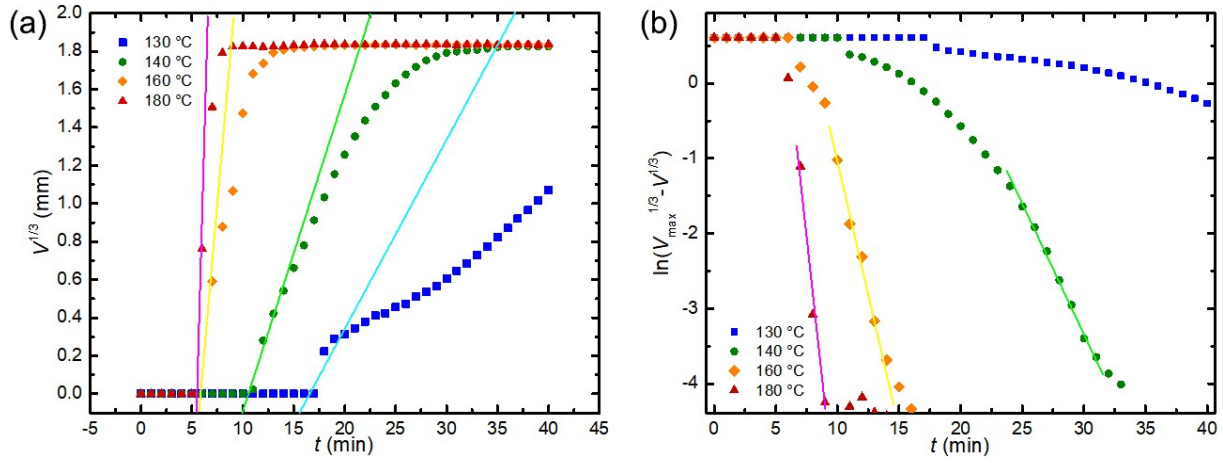

Figure S3. (a) The $V^{1/3} \sim t$ plot of the data shown in Fig. S2c for determining the initial guess of k by using the slope of linear fitting of data points at the very early growth stage according to eq. (S9). (b) The $\ln(V^{1/3}_{max} - V^{1/3}) \sim t$ plot of the data shown in Fig. S2c for determining the initial guess of D by using the slope of linear fitting of data points at the very late growth stage according to eq. (S10).

Table S1. The initial estimation of *k* and *D* values using the extreme-condition model for the synthesis at different temperatures.

Temp. /°C	$2\bar{r}_{max}$* /nm	N_0 /10^{12}	k /10^{-7} m·s^{-1}	*D* /10^{-14} m^2·s^{-1}	η*** /mPa·s
130	60	11	0.46	N/A**	1.99
140	103	11	0.78	0.15	1.79
160	116	7.5	2.7	3.92	1.44
180	143	4.0	6.75	21.7	1.21

([$AgNO_3$] = 0.10M [PVP] = 0.15M V_s = 6.0 mL)
*Calculated from the statistic average size measured from TEM images
**No available data for the very-late stage, using estimated $D = 0.07\times10^{-14}$ m^2·s^{-1} as initial guess.
***The viscosity of PVP-K30/EG solution are calculated from the Fikentscher's equation[3]:

$$\frac{\log(\eta_{rel})}{c} = \frac{75K_0^2}{1+1.5K_0c} + K_0$$

4th order Runge-Kutta method. Upon the implementation of the values of (*k*, *D*) pair, the nanoparticle growth trajectory ($r(t) \sim t$) can be calculated according to the full version LSW model (eq. S7). In order to numerically solve this autonomous ordinary differential equation ($\frac{dr}{dt} = r'(r,t)$), the classic 4th order Runge-Kutta method (RK4) with an initial condition $r(t_0)>0$ was applied. In RK4 method, once a point on the growth trajectory curve ($r(t_0) = r_0$) was given, the value on one stepwise after this point ($r(t_0+h)$) can be approximately represented by:

$$r(t_0+h) = r_0 + \frac{1}{6}h(k_1 + 2k_2 + 2k_3 + k_4) \quad \text{(S11)}$$

where k_1~k_4 are the slopes at the beginning, midpoints, and end point of this step:

$$\begin{cases} k_1 = r'(r_0, t_0) \\ k_2 = r'\left(r_0 + \frac{hk_1}{2}, t_0 + \frac{h}{2}\right) \\ k_3 = r'\left(r_0 + \frac{hk_2}{2}, t_0 + \frac{h}{2}\right) \\ k_4 = r'(r_0 + hk_3, t_0 + h) \end{cases} \quad \text{(S12)}$$

By repeating the RK4 method step after step, a series of points of $r(t+nh)$ (n = 1, 2, 3, …) can be numerically estimated. When the length of the step h is small enough, the numerical estimation of $r(t)$ curve converges to the analytical solution of the differential equation ($\frac{dr}{dt} = r'(r,t)$). The RK4 method can also be used backwards when the step length h is negative.

In this work, the starting point $r(t_0)$ was set to the midpoint of the growth curve where the first derivative (i.e., dV_{tot}/dt) reaches the maximum to minimize the relative error in determining the slope. The points before the midpoint were calculated by RK4 using $h = -1\times10^{-4}$ min and the points after that was calculated by using $h = 1\times10^{-4}$ min, which was much smaller than the temporal density of the experimental data points (1 point/min). The estimated $r(t)$ profile was converted to the total volume ($V_{tot}(t)$) profile using $V_{tot} = \frac{4}{3}N_0\pi r(t)^3$.

Simulated annealing algorithm. Once the value of a (k, D) pair is available, the data points estimated by RK4 (as V_{fit}) at the experimental time series (i.e., t=1, 2, 3, … min) were picked out to calculate the sum of squared residuals (*SSR*) with respect to the experimental data series (V_{exp}).

$$SSR = \sum_i \left|V_{fit}(t_i) - V_{exp}(t_i)\right|^2 \quad \text{(S13)}$$

A large *SSR* suggests a low-fidelity fitting of the input (k, D) pair while a small *SSR* indicates an appropriate fitting. Therefore, one can try as many (k, D) pairs as possible to find the best solution to fit the experimental data (so called Monte-Carlo method). However, such a completely random manner makes the computation process to be costly. The algorithm is improved by applying simulated annealing strategy, where the possibility of acceptance (P) of the new (k, D) pair is determined by the Metropolis's rule. A smaller *SSR* will be accepted immediately (P=1), and a larger *SSR* will be accepted conditionally:

$$P(k, D) = \begin{cases} 1, & SSR_{n+1} < SSR \\ \exp\left(-\dfrac{|SSR_{n+1} - SSR|}{R\tau}\right), & SSR_{n+1} \geq SSR \end{cases} \quad \text{(S14)}$$

R is a constant that only related to the efficiency of the algorithm and τ is the current "temperature" of the simulated annealing process that decreases after each iteration of searching. In our C-program, the simulated annealing algorithm is realized by the following iterations (described in plain text, note that all physical values including *k* and *D* are normalized to cancel the units to adapt the programming language):

1. τ = 100, *R*=0.01, (*k*, *D*) = (k_0, D_0) (initial guess evaluated from the extreme-condition model).
2. Calculate *SSR* using the RK4 method with the current (*k*, *D*) values.
3. Randomly pick a new (*k*, *D*) pair within the range of $k_{n+1} \in [k - \frac{\tau}{2}, k + \frac{\tau}{2}]$, $D_{n+1} \in [D - \frac{\tau}{2}, D + \frac{\tau}{2}]$.
4. Calculate SSR_{n+1} using the RK4 method with the current $(k, D)_{n+1}$ values.
5. Generate a random number *i* between 0 and 1.
6. Calculate the possibility of acceptance *P*(*k, D*)
    - If *P*(*k, D*) ≥ *i* (accepted)
        i. Save $(k, D)_{n+1}$ and SSR_{n+1} in memory as (*k*, *D*) and *SSR*, respectively.
        ii. Cool down the "temperature" $\tau = 0.99\tau$ (0.99 is the cooling rate)
        iii. Go to step 3.
    - If *P*(*k, D*) < *i* (rejected)
        i. Keep the old (*k*, *D*) and *SSR* in memory
        ii. Go to step 3.
7. Repeat steps 3-6 until $\tau < 0.1$
8. Print the (*k*, *D*), *SSR*, and the fitted $V_{fit}(t)$ in memory.

The computational parameters (τ_{max} =100, τ_{min} = 0.1, *R*=0.01, and the cooling rate 0.99) have already been optimized to achieve the convergency as well as to adapt the computational environments. Using these parameters, it only takes approximately 1 hour to run 100 independent

iterations on a laptop equipped with an Intel® Core™ i5-7200U processor. The computation can be accelerated by choosing a lower threshold of convergency (for example, a higher τ_{min} or a more rapid cooling rate) or coarsening the RK4 step length at the cost of the accuracy and stability of the output results or vice versa. However, due to the dice-rolling feature of the algorithm, the improvement on the output results, in a statistical manner, is not significantly affected by these parameters. A sample code of the C program attached with a brief instruction document can be found at Github: https://github.com/wsy94/NanoGK

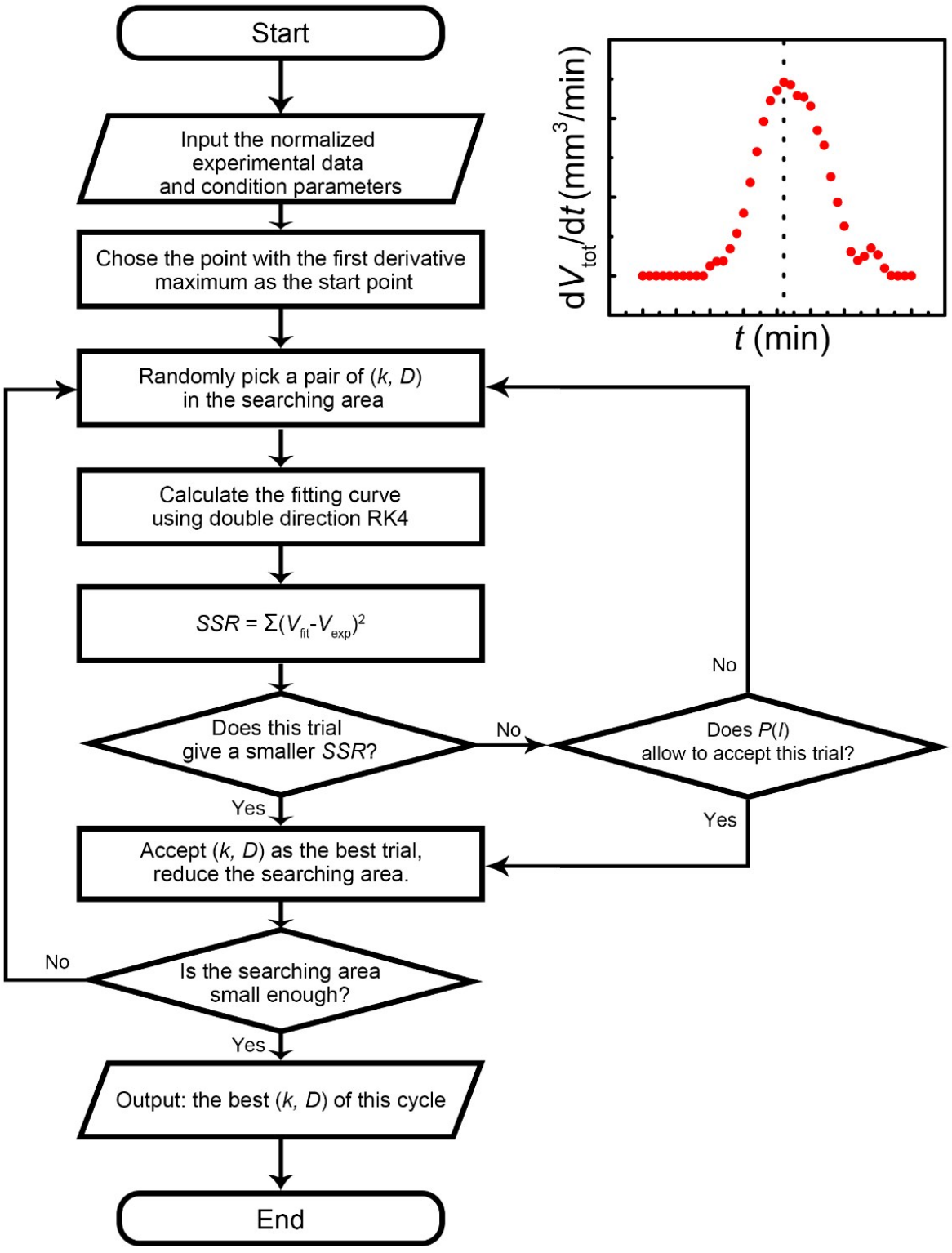

Figure S4. Flow chart of the simulated annealing algorithm. Insert: The maximum point at the first derivative function is chosen as the center for the two-way RK4 method.

Results of the simulated annealing algorithm.

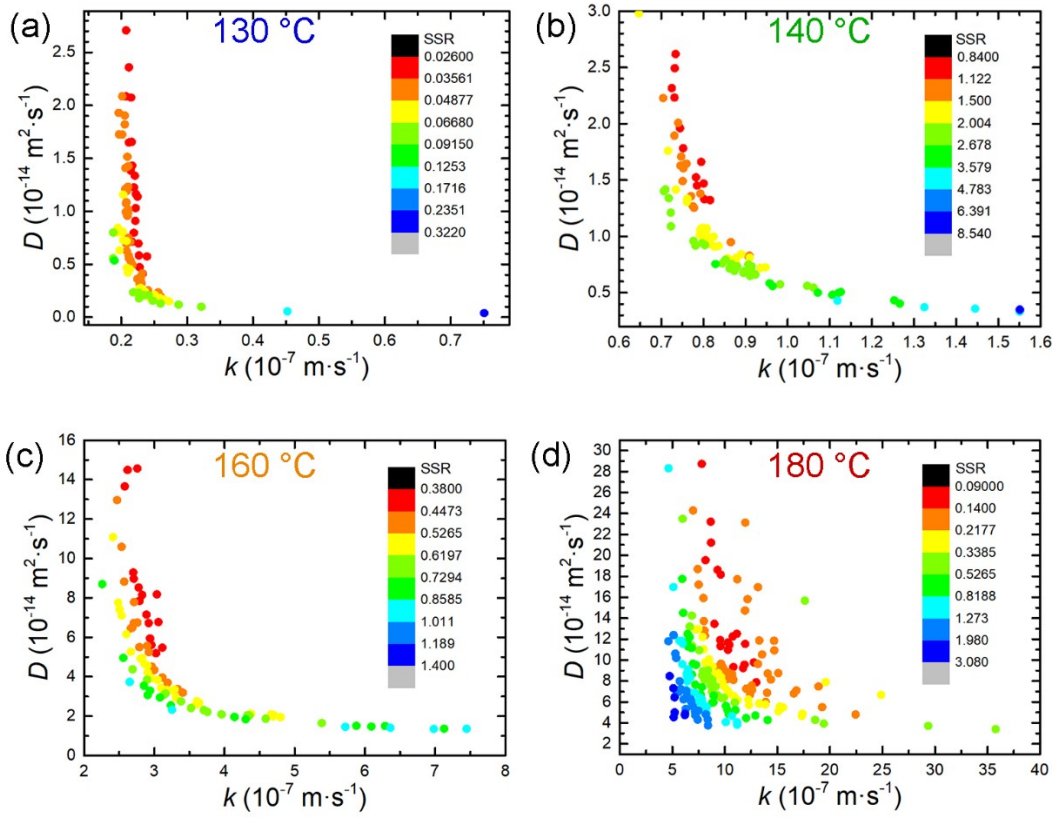

Figure S5. The optimized (*k*, *D*) pairs determined from the simulated annealing fitting of the growth kinetics of colloidal Ag nanoparticles measured from the syntheses at different temperatures: (a) 130°C, (b) 140°C, (c) 160 °C, and (d) 180 °C. The concentration of $AgNO_3$ was 0.1 M and the concentration of PVP in terms of repeat unit was 0.15 M. The colors of dots correspond to the *SSRs* calculated between the experimental data and the fitting data.

Table S2. Analysis on the fitted (*k*, *D*) values at different reaction temperatures*

Temp. /°C	trials	$\bar{k}$ /10^{-7} m·s^{-1}	$\sigma(k)$ /10^{-7} m·s^{-1}	$\bar{D}$ /10^{-14} m^2·s^{-1}	$\sigma(D)$ /10^{-14} m^2·s^{-1}
130	100	0.22	0.002	1.19	0.37
140	100	0.76	0.011	1.83	0.32
160	100	2.87	0.052	8.13	2.24
180	200	9.33	0.313	15.7	4.2

*Statistics are based on the top 10% best results.
Conditions: [$AgNO_3$] = 0.10M, [PVP] = 0.15 M, V_s = 6.0 mL

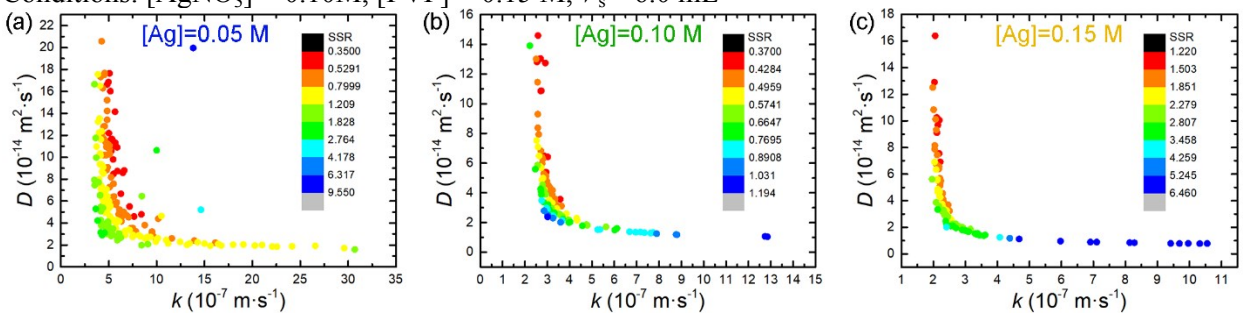

Figure S6. The optimized (k, D) pairs determined from the simulated annealing fitting of the growth kinetics of colloidal Ag nanoparticles measured from the syntheses at different $AgNO_3$ concentrations: (a) 0.05 M, (b) 0.10 M, and (c) 0.15 M. The temperature was 160 °C and the concentration of PVP in terms of repeat unit was 0.15 M. The colors of dots correspond to the *SSRs* calculated between the experimental data and the fitting data.

Table S3. Analysis on the output (k, D) values at different $AgNO_3$ concentrations*

[Ag] /M	$2\bar{r}_{max}$* /nm	N_0 /10^{12}	trials	$\bar{k}$ /10^{-7} m·s^{-1}	$\sigma(k)$ /10^{-7} m·s^{-1}	$\bar{D}$ /10^{-14} m^2·s^{-1}	$\sigma(D)$ /10^{-14} m^2·s^{-1}
0.05	110	5.54	200	6.21	0.31	10.65	3.04
0.10	116	9.45	100	2.85	0.09	9.68	2.75
0.15	123	11.89	100	2.12	0.02	10.23	1.93

*Statistics are based on the top 10% best results.
Conditions: T=160 °C, [PVP] = 0.15 M, V_s = 6.0 mL.

Section IV: Density functional theory (DFT) calculations on Ag-PVP complexes

Density functional theory (DFT) calculations. In the Ag-PVP system, the complex species of an Ag^0 or Ag^+ center coordinated with 1-2 of the repeating units (i.e., vinylpyrrolidone, VP) are used as the simplified models to reduce the computation time. The possible electron donor atom in VP can be the nitrogen atom and/or the oxygen atom. Both of the two cases are calculated. The calculations are all conducted at the ground state (i.e., the lowest possible multiplicity). The initial iteration of the geometry optimization is first optimized by molecular dynamics using MM3 method and then by B3LYP method[4,5] to achieve a higher-level accuracy. The standard relativistic effective core potential LanL2DZ basis set[6] is used for the metal center (i.e., Ag) involved in the calculation, while the other light atoms (H, C, N, O) of VP are calculated using the 6-31G(d) basis set.[7] The geometry and the B3LYP level energy of the last iteration of the geometry optimizations are adopted for discussion in this work. The calculation by B3LYP method using cc-pVDZ basis set[8] (on light atoms) and the calculation by MP2 method[9] at 6-31G(d) (on light atoms) are also performed for comparison. If the geometry optimization is not converging, for example, in calculating the transient states, single point energy calculations using the same geometry as either the non-ionic or ionic form are conducted. All of the calculations are performed on the WebMO 12.0 (WebMO, LLC) interface, which runs Gaussian 09™ (Gaussian, Inc.).

In a real synthesis of colloidal Ag nanoparticles, EG plays the roles of both solvent and reductant. In order to study the solvent effect, we consider the implicit model where the solvent molecules are treated as a polarizable continuous electric field.

The interaction between the metal center and the ligand can be described by the bond formation energy (E_{BF}), which is defined as the energy difference between the metal-ligand complex $\left(E\left(M-L_n\right)\right)$ and the sum of the energies of isolated metal center $E(M)$ and ligand molecules $E(L)$:

$$E_{BF} = E\left(M-L_n\right) - [E(M) - nE(L)] \qquad \text{(S15)}$$

where n is the number of ligand molecules that form coordination bond with the metal center. The reducibility of the metal ions or metal ion complex from the oxidation state to the corresponding reduction state are described by the first ionization energy, which is defined by the energy difference between the two states:

$$E_{IE} = E(M - L_n^+) - E(M - L_n) \quad \text{(S16)}$$

It is worth pointing out that E_{IE} is not same as the reduction potential due to the solvent effect. The calculations considering the solvent effect are also performed and discussed in this work, where the solvent (i.e., ethylene glycol) is treated implicitly as a polarizable continuous electric field.

Results and discussion from DFT calculations. In a synthesis of colloidal Ag nanoparticles, PVP is considered as a surfactant ligand that plays an important role of stabilizing the surface of nanoparticles and preventing aggregation of nanoparticles. PVP can also form complexes with metal precursor ions to influence the reaction kinetics.[10] A monomeric unit of PVP (VP) consists of a vinyl group and a 2-pyrrolidone ring containing a nitrogen atom and an oxygen atom as potential electron donors to the metal. To figure out the most stable coordination state in each case, we optimized the geometry and calculated the E_{BF} using VP as a model of the repeating unit. It is worthy to point out that the vinyl group in the monomer with two sp^2 C is substituted by the ethyl group with two sp^3 C, which has the closest structure to the polymerized hydrocarbon chain. The calculation results suggest that the coordination of Ag^+ to the oxygen atom (denoted by Ag^+-O-VP) of VP has the lowest E_{BF} (–38.3 kJ/mol) and the coordination of Ag^+ to the nitrogen atom (Ag^+-N-VP) has a less negative E_{BF} (–2.97 kJ/mol). Therefore, when $AgNO_3$ is dissolved in a EG solution that contains PVP, the free-standing Ag^+ ions tend to coordinate with the O atoms of the PVP ligand, forming a stable complex and lowering the actual concentration of ligand-free Ag^+. The Mulliken partial charge on Ag^+-O-VP is calculated to be +0.773, smaller than that of a freestanding Ag^+ cation (i.e., +1). The drop of the partial charge indicates that the electron donation of O atom enriches the electron density on Ag^+ and makes the reduction easier. The energy difference between the ionized Ag^+-O-VP and non-ionized Ag^0-O-VP is also smaller than that between Ag^+ and Ag^0, which agrees with the conclusion that the reduction of Ag^+-PVP costs less energy.

Once Ag^+ is reduced to Ag^0, the coordination bond between Ag and VP ligand is weakened in both the O bonded and N bonded configurations. The E_{BF} of Ag^0-O-VP is calculated to be 6.18 kJ/mol, as the distance between the Ag^0 atom and the electron donor (O atom) in the optimized geometries of Ag^0-O-VP is enlarged to 2.581 Å. The positive E_{BF} and the elongated coordination bond suggest that the PVP molecules is likely to interact with the reduced Ag^0 through physical adsorption rather than chemical bonding, enabling the continuous surface growth of Ag

nanoparticles. In a brief summary, the DFT calculations predict that the oxygen atom in the VP monomer is the most possible electron donor atom to coordinate with the Ag center. The conclusion agrees well with the experimental observation in the FTIR study[11] and the molecular dynamics simulation[12] reported in literature.

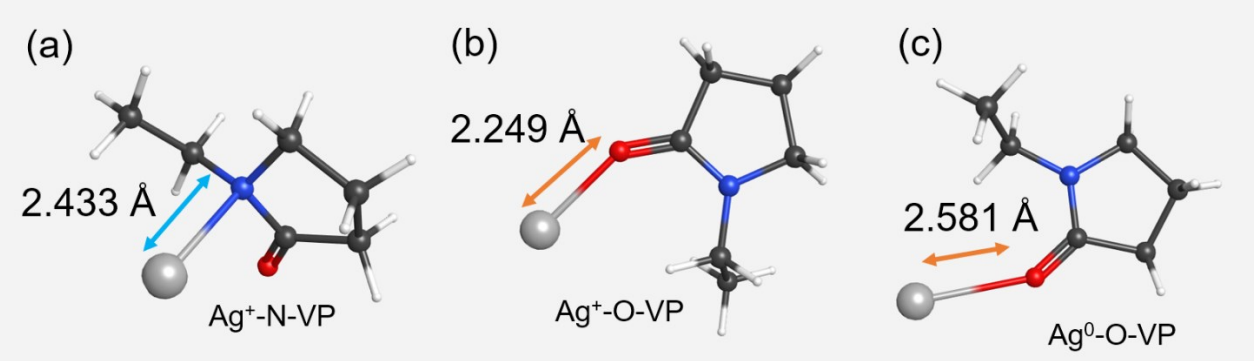

Figure S7. Optimized geometries of different coordination states: (a) Ag^+-N-VP, (b) Ag^+-O-VP, and (c) Ag^0-N-VP.

Having determined that the oxygen atom is the electron donor atom in a repeating unit of PVP, we step forward to study the case where Ag^0 or Ag^+ is coordinated with two repeating units $(VP)_2$, The calculation results are presented in Table S4 and compared in Figure S8. The geometry optimization of the two VP molecules results in a conformation where the two VP molecules are coordinates with the center Ag atom/ion in a linear geometry using the O atoms. The Ag^+-O bond length is 2.17Å in Ag^+-$(O\text{-}VP)_2$. The E_{BF} of the second Ag^+-(O-VP) bond is calculated as -60.6 kJ/mol, even more exergonic than forming the single-coordination complex Ag^+-(O-VP). The geometry optimization of the non-ionic Ag^0-$(O\text{-}VP)_2$ complex shows a longer Ag-O bond length of 2.68Å, indicating a weaker interaction between the atomic Ag^0 and the electron donors. The E_{BF} is 84.1 kJ/mol, indicating that forming the second coordination bond to Ag^0 atom is unlikely.

Table S4. DFT calculation results of various Ag-VP complexes using different methods.

Object	Units	LAND2DZ	B3LYP/6-31G(d)	B3LYP/cc-pVDZ	MP2/6-31G(d)
Ag^0	Hartree	-145.7611714			-144.9520879
Ag^+	Hartree	-145.6284244			-144.8618252
$E_{IE.0}$	Hartree	0.132747			0.090263
	kJ/mol	345.1421			234.6830
VP_1	Hartree		-365.2683355	-365.403344767	-364.0688884
Ag^0-VP	Hartree		-511.027129	-511.164864	-509.0125786
E_{BF}	Hartree		0.002378	-0.00035	0.008397638
	kJ/mol		6.1827	-0.90411	21.8339
Ag^+-VP	Hartree		-510.9114801	-511.0472711	-508.9314677
E_{BF}	Hartree		-0.01472	-0.0155	-0.000754119
	kJ/mol		-38.2722	-40.3049	-1.96071
$E_{IE.1}$	Hartree		0.115649	0.117593	0.081111
	kJ/mol		300.6872	305.7413	210.8884
Ag^0-VP_2	Hartree		-876.2631195	-876.5406506	-873.0372545
$E_{BF.2}$	Hartree		0.032345	0.027558	0.044212
	kJ/mol		84.09702	71.65121	114.95232
Ag^+-VP_2	Hartree		-876.203115809	-876.4745159	-873.0091584
$E_{BF.2}$	Hartree		-0.0233	-0.0239	-0.008802
	kJ/mol		-60.5806	-62.1399	-22.8861
$E_{IE.2}$	Hartree		0.060004	0.066135	0.028096
	kJ/mol		156.0096	171.9502	73.0500

The calculations based on B3LYP method using cc-pVDZ basis set (on light atoms) and the calculations based on MP2 method at 6-31G(d) (on light atoms) are also performed for comparison. The cc-pVDZ with a more complex basis set (compared to 6-31G(d)) has a higher accuracy but is more computationally expensive. The ground state energies, the bond formation energies (E_{BF}), and the ionization energies (E_{IE}) of each coordination state of Ag-VP complexes do not have a significant difference. The calculations from MP2, based on the many-body

perturbation theories, are much less accurate, with only the consistence on the orders of energies of different coordination states.

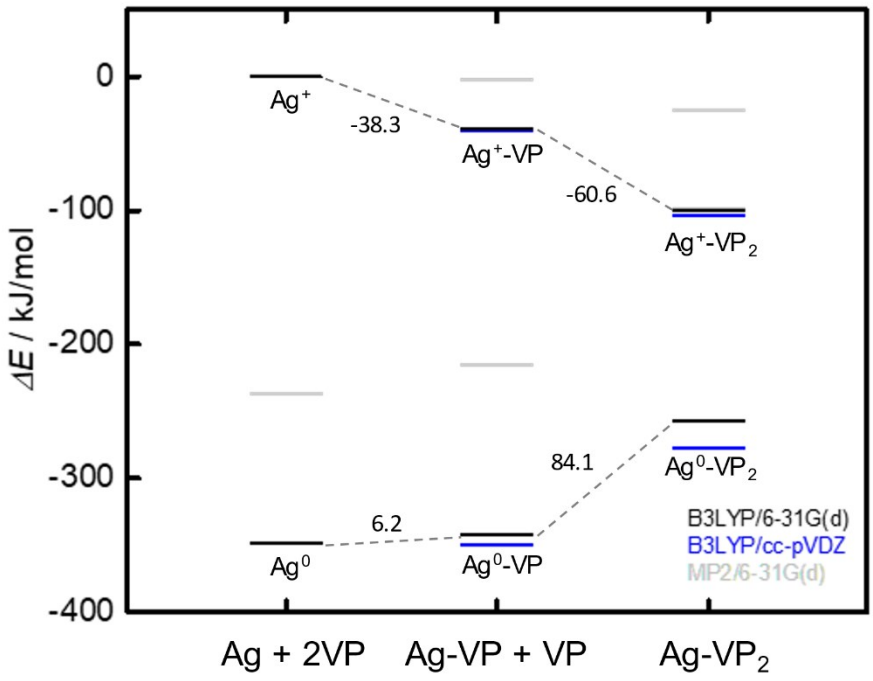

Figure S8. Energy diagram of various Ag-VP complexes calculated by DFT. The energy of freestanding Ag^+ cation is set as the reference zero.

The difference between the theoretical predictions and the experiment results can be attributed to several aspects. First, the implicit model does not include a sufficient amount of individual solvent molecules to mimic the actual condition, resulting in the deviation caused by missing the possible strong chemical interaction between the metal and solvent molecules. Second, the folding configuration of polymeric PVP and the partially charged double layer near the surface of the nanoparticles may cause the electronic structure of the metal complexes to be different from the simplified model between Ag and monomeric VP.

In conclusion, the actual Ag precursor species involved in the surface reduction reaction is Ag-(O-VP)$_n$ complex rather than all Ag(I) species that is used in the simulated annealing fitting. The difference between in the actual concentration of [Ag-(O-VP)$_n$] and the initial [$AgNO_3$] calculated

from the total $AgNO_3$ used for solution leads to the fitted *k* decreases as the amount of added $AgNO_3$ increases even at the same temperature.

Attachment: A sample input.com file for Gaussian 09 calculation of Ag^+-(O-VP)$_1$

```
#N B3LYP/GEN opt SCRF=(PCM,Solvent=1,2-EthaneDiol) pseudo=read
C6H11ONAg

1 1
C
C 1 B1
N 1 B2 2 A1
C 1 B3 2 A2 3 D1
C 1 B4 2 A3 3 D2
H 1 B5 2 A4 3 D3
H 1 B6 2 A5 3 D4
O 1 B7 2 A6 3 D5
Ag 1 B8 2 A7 3 D6
C 1 B9 2 A8 3 D7
C 1 B10 2 A9 3 D8
H 1 B11 2 A10 3 D9
H 1 B12 2 A11 3 D10
H 1 B13 2 A12 3 D11
H 1 B14 2 A13 3 D12
H 1 B15 2 A14 3 D13
H 1 B16 2 A15 3 D14
H 1 B17 2 A16 3 D15
H 1 B18 2 A17 3 D16
H 1 B19 2 A18 3 D17

B1 1.552505133
B2 2.392297513
B3 2.424886213
B4 1.549567337
B5 2.215055929
B6 2.227349722
```

B7 3.653601800

B8 5.793730781

B9 3.803138897

B10 4.481972894

B11 4.276944555

B12 5.526780967

B13 4.607342665

B14 4.153276921

B15 4.472971499

B16 2.217215908

B17 2.216749595

B18 1.092664195

B19 1.094558156

A1 37.17310470

A2 69.18803169

A3 104.3598295

A4 105.6116468

A5 124.0832490

A6 76.06952264

A7 68.31231653

A8 30.06414161

A9 35.09267052

A10 33.56452468

A11 31.51183987

A12 48.84051571

A13 17.61456029

A14 40.37504671

A15 27.08266753

A16 27.24902196

A17 111.5598494

A18 110.0068537

D1 7.876505743

D2 21.32231062

D3 49.52597281

D4 1.406312525

D5 6.833842453

D6 3.877243279

```
D7 -7.080223208
D8 -42.17335480
D9 -67.22589157
D10 -39.63171417
D11 -41.19945684
D12 14.57375060
D13 3.898030214
D14 -119.2412109
D15 117.9475921
D16 143.0927360
D17 -96.83604817

Ag 0
LANL2DZ
****
C H N O 0
6-31G(d)
****

Ag 0
LANL2DZ
```

References

(1) Liu, Q.; Gao, M. R.; Liu, Y.; Okasinski, J. S.; Ren, Y.; Sun, Y. Quantifying the nucleation and growth kinetics of microwave nanochemistry enabled by in situ high-energy x-ray scattering. *Nano Letters* **2016**, *16*, 715-20.

(2) Wu, S.; Sun, Y. An extreme-condition model for quantifying growth kinetics of colloidal metal nanoparticles. *Nano Research* **2019**, *12*, 1339-1345.

(3) Salamone, J. C., *Concise polymeric materials encyclopedia*. CRC press: 1998.

(4) Becke, A. D. Density-functional thermochemistry III: The role of exact exchange. *The Journal of Chemical Physics* **1993**, *98*, 5648-5652.

(5) Lee, C.; Yang, W.; Parr, R. G. Development of the Colle-Salvetti correlation-energy formula into a functional of the electron density. *Physical Review B* **1988**, *37*, 785-789.

(6) Wadt, W. R.; Hay, P. J. Ab initio effective core potentials for molecular calculations: potentials for main group elements Na to Bi. *The Journal of Chemical Physics* **1985**, *82*, 284-298.

(7) Ditchfield, R.; Hehre, W. J.; Pople, J. A. Self-consistent molecular-orbital methods IX: An extended Gaussian-type basis for molecular-orbital studies of organic molecules. *The Journal of Chemical Physics* **1971**, *54*, 724-728.

(8) Dunning, T. H., Jr. Gaussian basis sets for use in correlated molecular calculations I: The atoms boron through neon and hydrogen. *The Journal of Chemical Physics* **1989**, *90*, 1007-1023.

(9) Frisch, M. J.; Head-Gordon, M.; Pople, J. A. A direct MP2 gradient method. *Chemical Physics Letters* **1990**, *166*, 275-280.

(10) Sun, Y.; Xia, Y. Large-scale synthesis of uniform silver nanowires through a soft, self-seeding, polyol process. *Advanced Materials* **2002**, *14*, 833.

(11) Abdelghany, A.; Mekhail, M. S.; Abdelrazek, E.; Aboud, M. Combined DFT/FTIR structural studies of monodispersed PVP/gold and silver nanoparticles. *Journal of Alloys and Compounds* **2015**, *646*, 326-332.

(12). Mdluli, P. S.; Sosibo, N. M.; Mashazi, P. N.; Nyokong, T.; Tshikhudo, R. T.; Skepu, A.; van der Lingen, E. Selective adsorption of PVP on the surface of silver nanoparticles: a molecular dynamics study. *Journal of Molecular Structure* **2011**, *1004*, 131-137.